nature communications

Article

https://doi.org/10.1038/s41467-025-66213-w

The mantle source of REE-rich alkaline silicate magmas can be enriched by continent-derived sediment subduction

Received: 3 June 2025

Accepted: 3 November 2025

Published online: 17 December 2025

Check for updates

Kun-Feng Qiu[1] ✉, Zheng-Yu Long[2] ✉, Rolf L. Romer[3], Ralf Halama[4], A. E. Williams-Jones[5], Hao-Cheng Yu[1], Shan-Shan Li[1], Ming-Qian Wu[1] & Jun Deng[1,6] ✉

Alkaline silicate intrusions host large rare-earth-element (REE) resources, yet the precise origin of the mantle enrichment that generates these magmas remains unresolved. Here, we use a combination of Li-Ba-Sr-Nd isotopic data to clarify the processes responsible for the metasomatic enrichment of the mantle source. We focus on alkaline complexes in the North China Craton that host giant REE deposits, which exhibit broadly similar Li-Ba-Sr-Nd isotopic signatures, despite forming in different tectonic settings. Neither recycling of altered oceanic crust nor serpentinite-related metasomatism can reproduce these coupled geochemical signatures; instead, they require the addition of subducted continent-derived sediment derived from weathered continental crust. Storage of these REE-rich sediments within the lithospheric mantle lowers its solidus and creates chemically fertile domains. Lithospheric extension subsequently triggers selective melting of these domains, generating REE-rich alkaline magmas. Our findings suggest that continent-derived sediment recycling plays an important role in shaping the critical-metal budget of the Earth.

Alkaline igneous rocks, which commonly occur along craton margins (Fig. 1A), host ~30% of global rare earth element (REE) resources. The REE-rich alkaline complexes are generally considered to form from low-degrees of partial melting of the sub-continental lithospheric mantle (SCLM) that is highly enriched in REEs, alkali elements, and volatiles[1–3]. This enrichment is commonly attributed to metasomatism by slab-derived fluids/melts that introduce volatiles and REEs[4–7], with plate subduction thought to play a critical role[1,2]. Despite broad agreement that the source enrichment of alkaline rocks is subduction-related, there is no consensus on the nature of the subducted material[1,2]; whether it is derived primarily from marine sediment or altered oceanic crust (AOC)[2,6,8–12]. Moreover, the "marine sediment" end-member is intrinsically heterogeneous, comprising mixtures of oceanic authigenic phases with continent-derived detrital minerals. Furthermore, recycled materials can be stored at subsolidus conditions in the SCLM for hundreds of millions of years[13–17] before being remobilized by tectonic events that trigger mantle remelting and generate alkaline magmas[18]. This implies that recycled material may have been introduced into the SCLM through multiple subduction events.

Element partitioning during slab subduction controls which elements are transferred to the mantle. Aqueous fluids released by slab dehydration do not mobilize high-field-strength elements (HFSE) and REEs in significant amounts[19], whereas partial melting of the

[1]State Key Laboratory of Geological Processes and Mineral Resources, Frontiers Science Center for Deep-time Digital Earth, School of Earth Sciences and Resources, China University of Geosciences, Beijing, China. [2]Université Paris Cité, Institut de Physique du Globe de Paris CNRS, Paris, France. [3]GFZ Helmholtz Centre for Geosciences, Telegrafenberg, Potsdam, Germany. [4]Institute of Geosciences and Geography, Martin-Luther-University Halle-Wittenberg, Halle (Saale), Germany. [5]Department of Earth and Planetary Sciences, McGill University, Montreal, QC, Canada. [6]Geological Research Institute of Shandong Gold Group Co. Ltd., Jinan, China. ✉e-mail: kunfengqiu@qq.com; long@ipgp.fr; djun@cugb.edu.cn

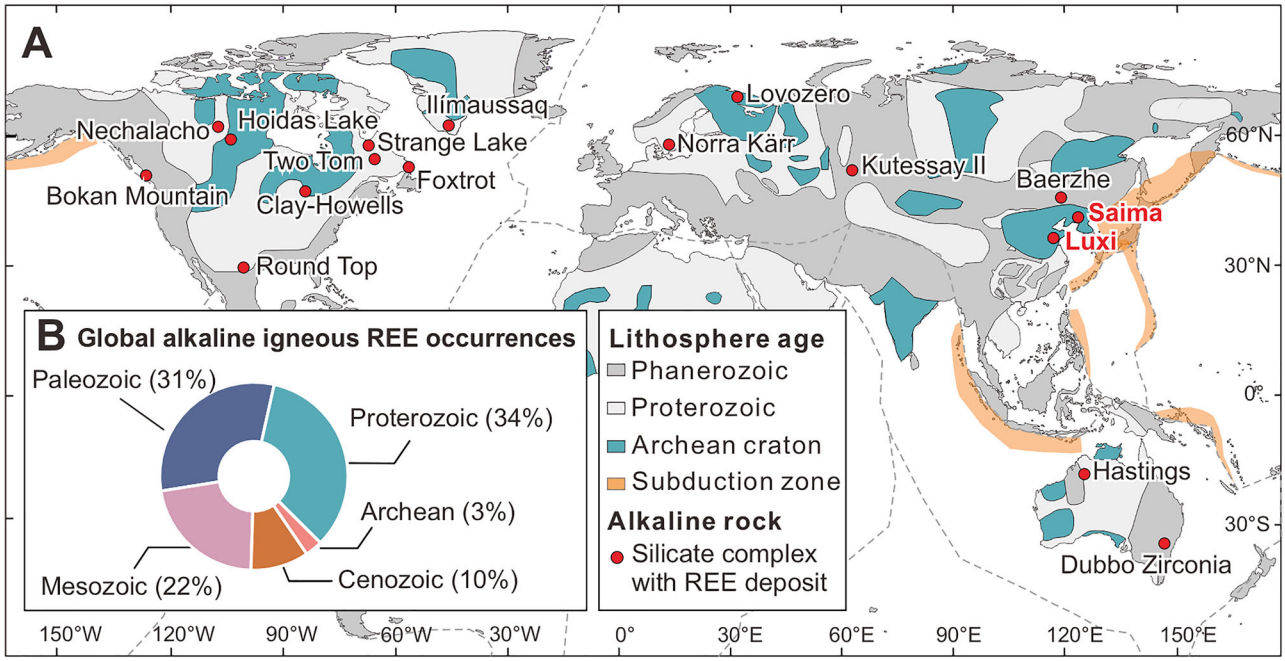

Fig. 1 | The global distribution and temporal occurrence of alkaline igneous REE deposits. The global distribution of major alkaline igneous REE deposits (**A**) was adapted from the USGS report[92]. Also shown is the distribution of global alkaline igneous REE occurrences across major geological eras (**B**), based on the USGS database[93].

subducting slab can transport REEs and even some HFSEs[20]. These slab-derived agents percolate into and react with the overlying mantle, crystallizing distinctive metasomatic mineral assemblages that sequester the introduced elements into enriched veins or pockets[21–23]. Typical products include phlogopite and amphibole, which host Li, Ba, K, and REEs, together with clinopyroxene enriched in light REEs[21–23]. Subsequent partial melting of this metasomatized mantle generates alkaline magmas that inherit the chemical fingerprints of these metasomes[22,24]. Incompatible elements, Li, Ba, and REEs partition preferentially into the melt during mantle melting. Thus, the enrichment of Li and Ba is directly linked to that of the REEs from mantle source enrichment to magma generation.

In this context, Li and Ba and their isotopes (δ^7Li and $\delta^{138/134}$Ba) serve as sensitive tracers for identifying the sources of REE-rich alkaline rocks and distinguishing contributions from different recycled reservoirs. The depleted mantle has relatively restricted δ^7Li and $\delta^{138/134}$Ba values, as inferred from fresh MORB (e.g., δ^7Li = +3.5 ± 1.0 ‰; $\delta^{138/134}$Ba = +0.03 to +0.05‰)[25,26]. In contrast, sediments and altered oceanic crust display wider ranges in Li and Ba isotopic compositions, generally overlapping but collectively spanning δ^7Li = −5 to +20‰[25,27,28] and $\delta^{138/134}$Ba = −0.21 to +0.40‰[29–31]. Addition of Li and Ba from slab-derived materials can partially modify the isotopic composition of the lithospheric mantle, with the shift depending on the nature of the subducted source[24,31]. Altered oceanic crust and oceanic authigenic sediments typically impart heavier Li and Ba isotopic compositions, whereas continent-derived sediments are generally lighter (see Discussion). Consequently, the δ^7Li and $\delta^{138/134}$Ba values of the lithospheric mantle will tend to increase where enrichment reflects subducted oceanic crust and authigenic sediments, and decrease where continent-derived sediments are incorporated[24,32–34].

There are numerous alkaline intrusions within the North China Craton (NCC), several of which host notable REE mineralization. Particularly important are the alkaline igneous complexes in the Luxi REE belt and the Saima REE-Nb-Ta deposit at the eastern margin of the NCC (Supplementary Fig. S1). Previous radiogenic and oxygen isotope studies have provided evidence of significant crustal contributions to the mantle sources of these alkaline rocks[35–37]. Despite geochemical similarities, the tectonic settings that triggered SCLM melting differ. The NCC has experienced four tectono-thermal events since the Paleozoic. These are: 1) the southward subduction of the Paleo-Asian oceanic plate beneath the NCC during the late Carboniferous to Late Permian; 2) the closure of the Proto-Tethys along the Qinling-Dabie belt in the Devonian; 3) the thrusting of Yangtze crust beneath the NCC during the Late Permian to Late Triassic along the Dabie-Sulu orogenic belt; and 4) the subduction of the Izanagi (Paleo-Pacific) plate beneath the eastern NCC during the Jurassic and Early Cretaceous[38]. At Luxi, the magmas (130–120 Ma) were generated during the rollback and steepening of the Izanagi slab, whereas magmatism at Saima (231–224 Ma) is associated with post-collisional crustal extension[35–37]. Detailed descriptions of the Luxi and Saima deposits and the analyzed samples are provided in the Supplementary Material.

In this work, we report Li-Ba-Sr-Nd isotope data for the Luxi and Saima alkaline complexes (sample information in Supplementary Table S1) to show that the mantle became metasomatized before sourcing the giant REE-bearing alkaline rocks. Our results provide compelling evidence that recycling of continent-derived sediments exerts a primary control on the mantle enrichment that ultimately generates the REE-bearing alkaline magmas, implying a similar petrogenesis for regions elsewhere that host large REE deposits.

Results and discussion

Analytical results

The alkaline rocks from the Luxi REE belt and the Saima complex have contrasting major element compositions; most importantly, they differ in their contents of SiO_2, Al_2O_3 and total alkali elements (Supplementary Fig. S2). Those from Luxi vary considerably in composition, with SiO2 contents ranging from 58.9 to 70 wt.%, but for one sample that contains 75.3 wt.% SiO_2, $Na_2O + K_2O$ from 7.36 to 12.1 wt.%, and Al_2O_3 from 11.9 to 16.2 wt.%. Although most of the rocks are classified as syenites based on their mineralogy (Supplementary Table S2), a few samples fall in the granite, granodiorite, and monzonite fields on a TAS diagram (Supplementary Fig. S2). The Luxi rocks are transitional between alkaline and subalkaline compositions (Supplementary Fig. S2). Despite the variation in major element composition, the subalkaline and alkaline rocks from the Luxi belt have similar primitive mantle-normalized trace-element signatures, characterized by

https://doi.org/10.1038/s41467-025-66213-w

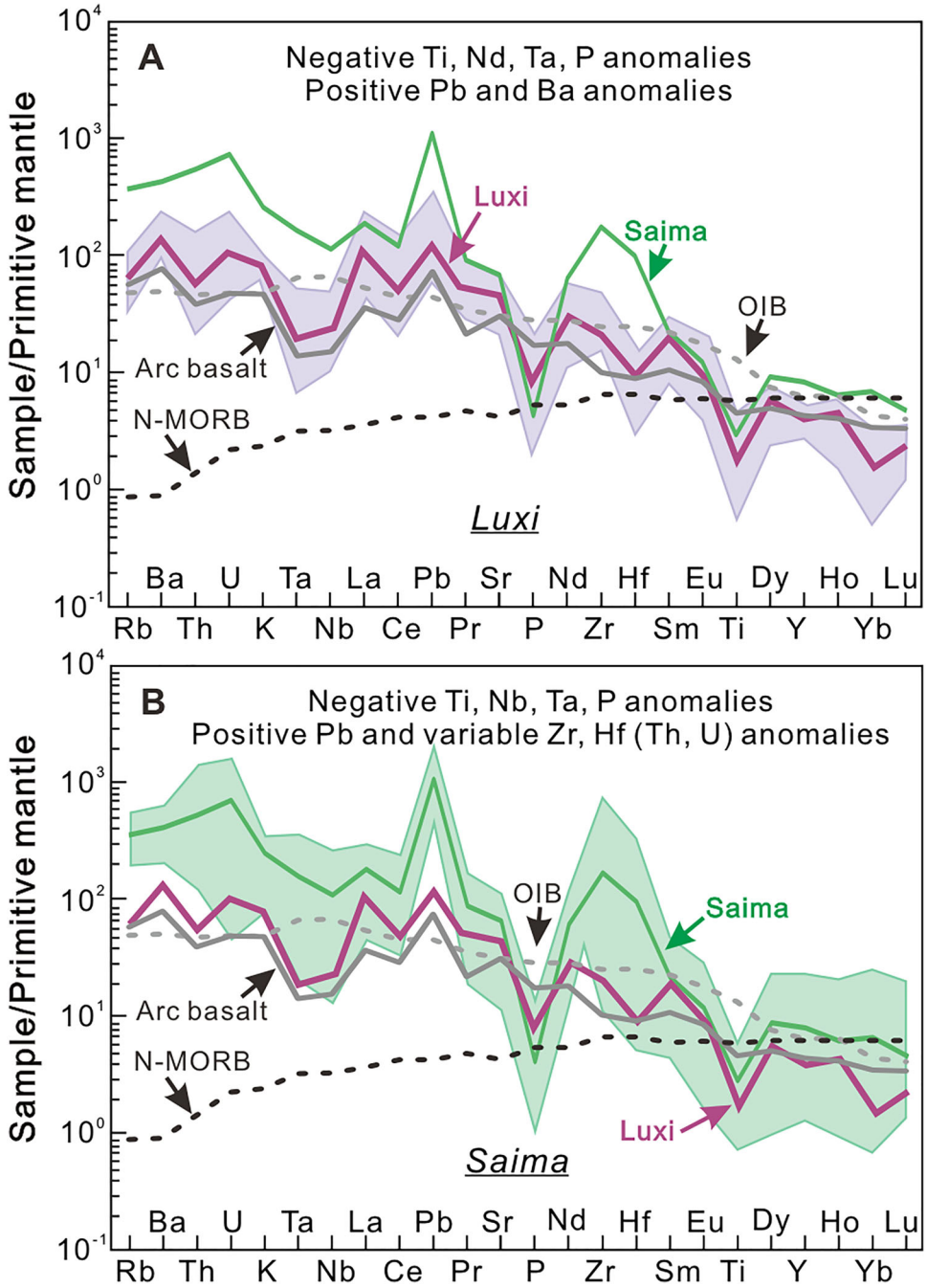

Fig. 2 | Primitive-mantle-normalized trace-element profiles of alkaline rocks from Luxi and Saima. A Luxi; **B** Saima. Purple curves = Luxi; green curves = Saima. The shaded envelopes (purple in (**A**), green in (**B**)) denote the full range of values for individual samples, and the central bright line is the arithmetic mean for the samples. Reference curves for ocean-island basalt (OIB; gray dashed), arc basalt (gray solid), and depleted mid-ocean ridge basalt (N-MORB; black dotted) are shown for comparison. The primitive-mantle values are from the reference[94].

enrichments in LREEs, LILEs (e.g., Sr, Ba, and Pb) and depletions in Ti, Nb, Ta, and P, as well as in the HREEs relative to LREEs (Fig. 2A). The Li contents of these rocks range from 1.8 to 108 ppm and the δ^7Li values from −4.6‰ to +4.8‰ (Fig. 3A). The Luxi alkaline rocks generally have high Ba contents (from 1436 to 4573 ppm) and variable $\delta^{138/134}$Ba values, ranging from −0.26‰ to +0.13‰ (Fig. 3B). The alkaline rocks are characterized by relatively high initial Sr isotope ratios ($^{87}Sr/^{86}Sr_{(130)}$ = 0.7068–0.7112) and low Nd isotope ratios ($\varepsilon Nd_{(130)}$ = − 15.65 to −7.63) (Fig. 4).

Alkaline rocks from the Saima complex have lower SiO_2 contents (57.4–63.4 wt.%), higher $Na_2O + K_2O$ contents (10.9–15.4 wt.%) than those of the Luxi belt, and similar Al_2O_3 contents (13.4–17.0 wt.%). They plot in the syenite and foid syenite fields in the TAS diagram (Supplementary Fig. S2). The Saima alkaline rocks commonly have higher trace element contents and more variable trace-element signatures than the Luxi rocks. The primitive mantle-normalized trace-element profile of the Saima samples shows distinct positive Pb anomalies and negative P and Ti anomalies (Fig. 2B). Some samples also display distinctly negative Nb and Ta anomalies, which is typical for subduction-modified mantle rocks, whereas other samples exhibit no Nb and Ta anomalies. Similarly, some samples show positive U and Th anomalies and enrichments of Zr and Hf relative to LREE, whereas other samples

https://doi.org/10.1038/s41467-025-66213-w

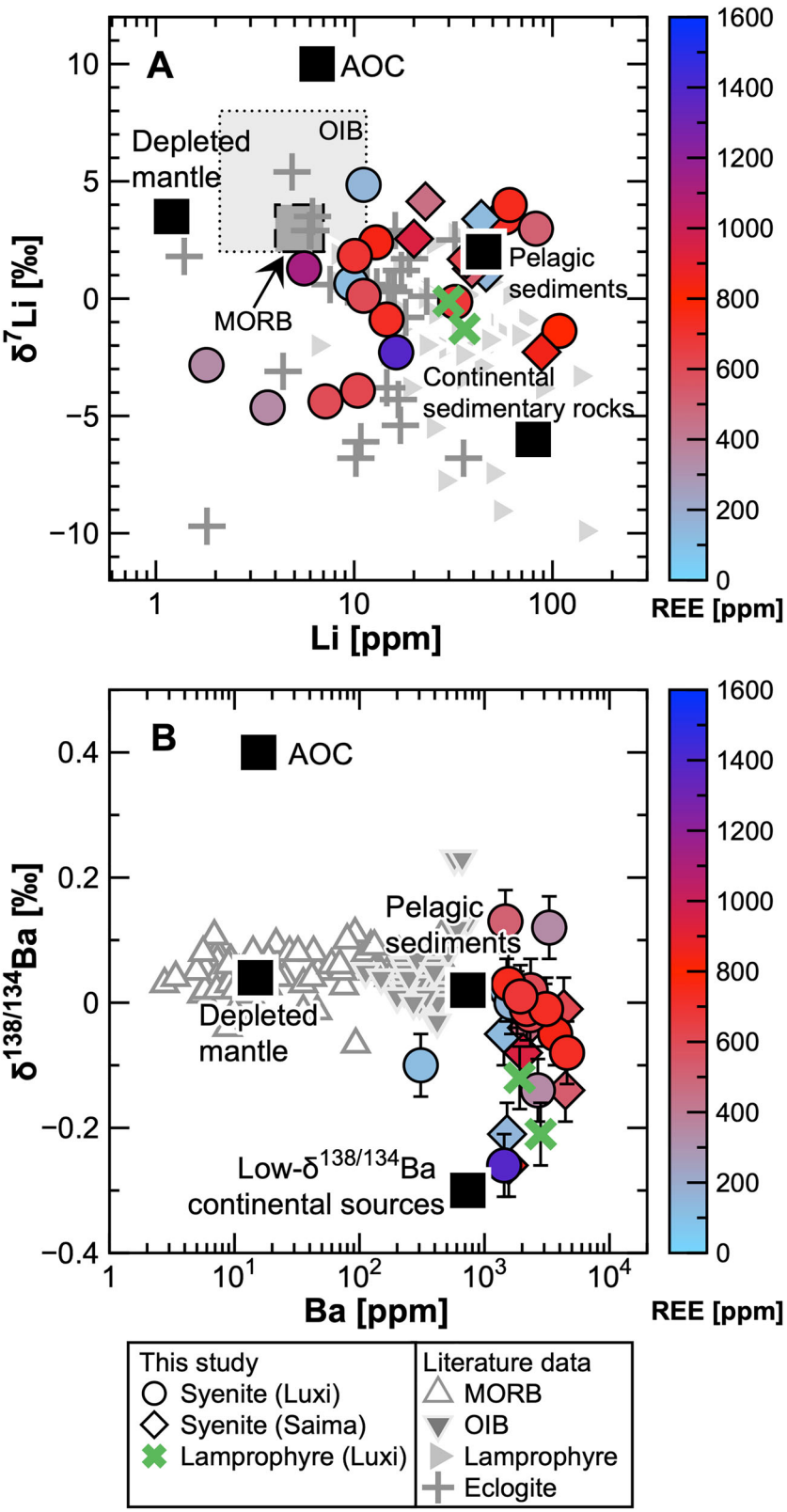

Fig. 3 | Lithium and Ba isotope ratios versus concentration for samples from this study and the literature. A δ^7Li vs. Li content, **B** $\delta^{138/134}$Ba vs. Ba content. The color ramp on the right side varies in color intensity, corresponding to the REE concentration in the samples. The error bars show the 2 SD uncertainties of the $\delta^{138/134}$Ba measurements. For δ^7Li, they are smaller than the symbol size. The δ^7Li and $\delta^{138/134}$Ba values of the depleted mantle were taken to be +3.5 ± 1.0 ‰[25] and +0.03 to 0.05‰[26], respectively. The AOC typically displays heavier Li and Ba isotope compositions, e.g., δ^7Li up to +10‰; $\delta^{138/134}$Ba up to +0.40‰[25,31]. Globally, subducted sediments have highly variable δ^7Li values, mostly from −4.3 to +14.5‰[27]. Pelagic sediments have $\delta^{138/134}$Ba values ranging from −0.21 to +0.13‰, equal to or slightly lighter than the mantle values[29–31]. AOC altered oceanic crust, UCC upper continental crust. The data sources are as follows: MORB[31,55,95], OIB[25,43,96], weathered basalt[60], eclogite[54,55], amphibolite[54], and lamprophyres from the Bohemian Massif[24].

https://doi.org/10.1038/s41467-025-66213-w

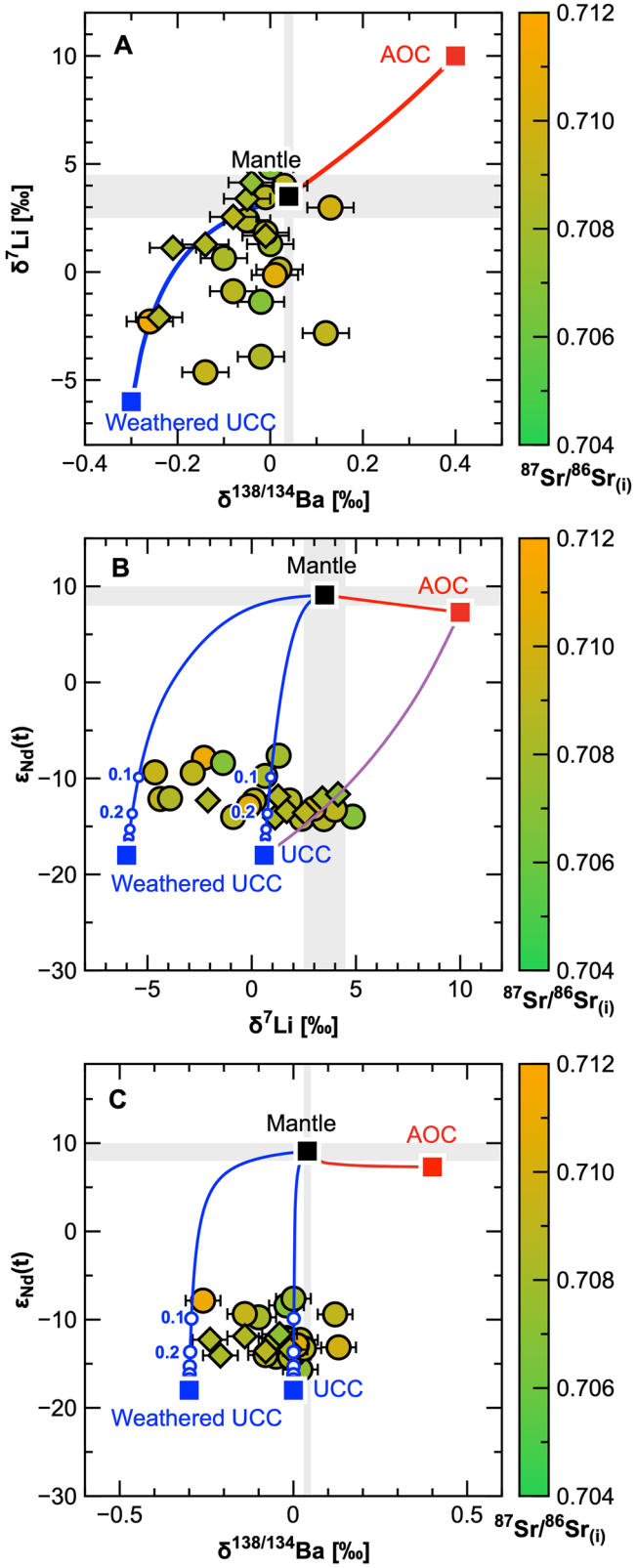

Fig. 4 | The Li-Ba-Sr-Nd isotopic ratios of the investigated alkaline rocks. A δ^7Li vs. $\delta^{138/134}$Ba, **B** $\varepsilon_{Nd}(t)$ vs. δ^7Li, and **C** $\varepsilon_{Nd}(t)$ vs. $\delta^{138/134}$Ba. The sample symbols are as in Fig. 3. The color ramp on the right side varies in color intensity, corresponding to the $^{87}Sr/^{86}Sr_{(i)}$ ratio in the samples. The error bars show the 2 SD uncertainties of $\delta^{138/134}$Ba measurements. The error bars of δ^7Li and $\varepsilon_{Nd}(t)$ are smaller than the symbol size. The numbers along the mixing curves show the mixing proportions. The gray-shaded region represents the range of the mantle. See Supplementary Table S6 for the additional parameters used in the mixing modeling.

have negative U and Th anomalies and are depleted in Zr and Hf relative to LREE. The alkaline rocks from Saima have Ba and Li contents ranging from 1431 to 4440 ppm and from 20 to 88 ppm, respectively (Fig. 3). The $\delta^{138/134}$Ba values range from −0.22‰ to +0.01‰ and the δ^7Li values range from −2.2‰ to +4.1‰ (Fig. 3). The alkaline rocks have relatively radiogenic initial Sr isotope ratios ($^{87}Sr/^{86}Sr_{(230)}$ = 0.7072–0.7086) and relatively low Nd isotope ratios ($\varepsilon Nd_{(230)}$ = −14.1 to −11.7) (Fig. 4). The two groups of alkaline rocks from Saima, i.e., the foid-syenites and the syenites, have similar ranges of Ba, Sr, and Nd isotope compositions.

Some of the Luxi samples display highly negative δ^7Li values, whereas others display MORB-like positive δ^7Li values. Most of the Saima rocks have positive δ^7Li values, but one sample has a highly negative δ^7Li value (Fig. 3A). As is the case for some arc magmas, the δ^7Li values (−4.64 to +4.85‰) are mostly lighter than those of depleted mantle; the $\delta^{138/134}$Ba values (−0.26 to +0.13‰) are also lighter (Fig. 3B). The contents of Li and Ba do not correlate with the isotopic compositions of the corresponding elements. These samples, collectively, have high $^{87}Sr/^{86}Sr_{(t)}$ ratios (0.7068–0.7129) and low $\varepsilon_{Nd}(t)$ values (−15.6 to −7.6) (t = 130 Ma for Luxi samples and 230 Ma for Saima samples) (Fig. 4), deviating from the mantle array. For comparison, calc-alkaline lamprophyres from Luxi have δ^7Li values in the range of −1.3 to −0.1‰, i.e., lower than those of MORB and OIB but within the middle of the range for the alkaline rocks (Fig. 3A).

The REE contents of the samples, although elevated (the color ramp in Fig. 3), do not reach ore grade (typically 0.4–1.4 wt% TREO[39]; Total Rare Earth Oxide). In alkaline complexes, economic REE mineralization commonly results from late-stage processes (advanced differentiation and hydrothermal alteration) that can concentrate REEs by orders of magnitude relative to the parental magmas[40,41]. Because these processes can also perturb Li and Ba isotope ratios (see Supplementary Material), we targeted less-evolved, fresh rocks from the Luxi and Saima suites to characterize their primary geochemical signatures.

Recycled continent-derived material dominates the source of REE-rich syenite magmas

The Li-Ba-Sr-Nd isotopic compositions of the investigated alkaline complexes reflect their mantle source, since these compositions cannot be explained by partial melting, magmatic differentiation, crustal assimilation, or surface alteration and weathering (see discussion in the Supplementary Material). Alkaline rocks from Luxi and Saima have low δ^7Li, $\delta^{138/134}$Ba, and $\varepsilon_{Nd}(t)$ values, as well as high $^{87}Sr/^{86}Sr_{(t)}$ values, clearly deviating from depleted mantle compositions but closely resembling the signature of slab lithologies introduced into the lithospheric mantle (Figs. 3 and 4).

Evidence of recycled materials in Luxi and Saima alkaline rocks. Additions from subducted slab materials are also apparent from the arc-like trace-element patterns (Fig. 2) and elevated Th/Yb and Nb/Yb ratios compared to the MORB array (Supplementary Fig. S6). An excess of Th relative to Nb and Yb is often interpreted to indicate a sediment or continental-crust contribution, since Th is enriched in the continental crust and sediment[42]. Thus, the geochemical characteristics suggest recycled materials in the mantle source. In subduction zones, forearc serpentinites typically have low concentrations of Li and Ba[25,31]. As a result, any fluid released from serpentinites would have only a minor effect on the Li and Ba isotopic composition of the overlying mantle. In addition, although a substantial fraction of slab-hosted Ba and Li is released at sub-arc depths, a non-negligible portion can be retained and recycled into the convecting mantle, as indicated by the near-mantle $\delta^{138/134}$Ba in OIB (HIMU only up to +0.11‰; EM only down to

−0.07‰)[43] and the slightly elevated Li isotopic compositions of OIBs (Fig. 3). Nevertheless, the small magnitude of these deviations implies that such recycled inputs have a limited ability to modify the deep mantle and are unlikely to account for the isotopic features of our samples. Importantly, large peralkaline complexes that formed in plume settings (e.g., in the Kola Peninsula, Russia) typically have depleted Sr and Nd isotope ratios (low initial 87Sr/86Sr and positive εNd(t) values) consistent with their derivation from a mantle that has been long depleted[44], whereas the NCC alkaline complexes have enriched lithospheric signatures (negative εNd(t); elevated initial 87Sr/86Sr; Fig. 4), indicating a lithospheric source. Thus, the possibility of a significant contribution from the deep mantle can be ruled out. In fact, most of the subducted Li and Ba are sequestered in the SCLM (creating an enriched slab-influenced domain)[45]. The Luxi and Saima magmas likely originated from this enriched SCLM beneath the craton.

Minor influence of altered oceanic crust. Subducted altered oceanic crust has often been considered a potential source of trace element enrichment in mantle-derived magmas[9,12,46,47]. Altered oceanic basalts and oceanic authigenic sediments typically acquire heavy Li and Ba isotope signatures due to interaction with seawater[48,49]. Modern seawater is highly enriched in heavy Li (δ^7Li up to +31‰) and heavy Ba ($\delta^{138/134}$Ba up to +0.6‰)[25,31]. Consequently, oceanic crust altered at low temperature can record very elevated δ^7Li (often reaching +10 to +20‰)[25] and moderately high $\delta^{138/134}$Ba[31] values (Fig. 3). If melts or fluids derived from such AOC were added to the mantle source beneath Luxi and Saima, it is expected that the metasomatized mantle would have shifted toward heavier Li and Ba isotopic compositions[25,32,50]. This effect would even be enhanced if equilibrium isotope fractionation during fluid formation occurred, since for both isotope systems, the heavy isotope is preferentially incorporated into the fluid[51,52]. Additionally, low δ138/134Ba values (−0.22 to −0.06‰) have been reported for several lower-oceanic-crust samples[53]. These samples, however, contain very little Ba (6.5–8.0 ppm), substantially less than MORB, and therefore, such a Ba-poor source cannot explain the positive Ba anomalies (i.e., high Ba contents) that are characteristic of alkaline rocks (Fig. 2).

Several lines of evidence indicate that AOC alone cannot account for the isotopic compositions observed in the alkaline rocks. Firstly, dehydration reactions in the oceanic crust drive the heavier Li and Ba isotopes into the fluid phase, leaving the residual slab depleted in heavy isotopes[51,54,55]. Thus, when the AOC reaches sub-arc depths, it may no longer carry a heavy isotopic signature as much of the heavy Li and Ba may have been lost to fluids that escaped into the forearc. Slab dehydration can cause at most a 2–4‰ decrease in the δ^7Li of the residual slab[55], which would not be sufficient to produce the much lower δ^7Li values (down to −4.6‰) recorded in some samples. Moreover, if slabs are stripped of heavy Li and Ba by fluid release, they would retain only minor amounts of these elements, which in turn are unlikely to significantly affect the source magmas of the alkaline rocks. Secondly, the AOC typically has positive εNd(t) values because its Nd isotopic composition remains similar to that of MORB even after alteration. In contrast, the Luxi and Saima rocks have strongly negative $\varepsilon_{Nd}(t)$ values (Fig. 4). This signature is more consistent with old continental crust than with young oceanic crust. Finally, if pelagic (deep-sea) sediments or AOC were the dominant contributors of REEs and other metasomatic components, one might expect heavier Li and Ba isotopic compositions in the resulting magmas[31,56]. Instead, the data show the opposite (lighter), ruling out a simple AOC-dominated source.

Dominant influence of subducted continent-derived sediments. Our data suggest that continent-derived sediments are the principal source of the unusually light Li and Ba isotope signatures in the Luxi and Saima mantle. Unlike pelagic sediments or AOC, continent-derived sediments have intrinsically low δ7Li and δ138/134Ba[28], which can be imparted to the mantle when these sediments are subducted and release fluids or melts[24,31]. Siliciclastic sediments from continental crust typically carry the isotopic imprint of chemical weathering and erosion. During weathering on the continents, secondary minerals (like clays) preferentially take up the lighter isotope ^{6}Li, while ^{7}Li is leached into fluids[57]. This leaves the weathered rock and soils depleted in ^{7}Li and thus characterized by low δ^7Li values (e.g., down to −6.8‰ in weathered granites)[58]. Moreover, diagenesis and prograde metamorphism of sediments in the subduction environment can further lower their δ7Li values by driving off ^{7}Li-rich fluids[59], yielding residual solid phases with lower δ7Li values. Barium isotopes behave similarly. Thus, continental sediments are a potentially light $\delta^{138/134}$Ba reservoir, because weathering and metamorphic dehydration both remove ^{138}Ba from the rocks[51,60].

In general, metasomatic agents derived from these sediments will have lower δ^7Li and $\delta^{138/134}$Ba values, especially if the sediment has undergone prior slab dehydration. This creates a heterogeneous SCLM for later alkaline magmatism. The data cluster toward the light end of δ^7Li-δ^{138}Ba space and overlap the isotopic signatures of continent-derived sediments, and together with the negative $\varepsilon_{Nd}(t)$ and high $^{87}Sr/^{86}Sr_{(t)}$ values, indicate that continent-derived sediment was the dominant metasomatic agent.

Isotopic mixing models of crustal recycling. The variable ranges of δ^7Li and $\delta^{138/134}$Ba values in the samples reflect the heterogeneous nature of the source. Subducted slabs are compositionally diverse, ranging from relatively heavy (marine chemical sediments or AOC-influenced) to very light (weathered continental detritus-dominated)[27–30]. To quantify the proportion of recycled material, mixing models have been developed using representative end-member compositions. One end-member is the mantle (SCLM) and the other end-members correspond to two distinct continental crustal materials: (i) an average upper continental crust (UCC) with δ^7Li = +0.6 ± 0.6 ‰ and $\delta^{138/134}$Ba = 0.00 ± 0.04‰[57,61] (this "normal" UCC reflects limited weathering/metamorphism); and (ii) a highly weathered or dehydrated crustal component with much lighter isotope ratios (set as δ^7Li = −6‰ and $\delta^{138/134}$Ba = −0.3‰). These values, for the light end-member, represent the materials from continental shales, weathered granites, and metamorphosed sediments. Details of the modeling are provided in the Supplementary Material.

The modeling results indicate that an addition of 10–20% of sediment or crustal material is required in the mantle source to account for the isotopic compositions observed in the Luxi and Saima alkaline magmas (Fig. 4). In Li-Ba isotope space, the data for the alkaline rocks plot between the mixing trajectories of mantle-UCC and mantle-weathered UCC mixtures, rather than along the mantle-AOC line. This suggests that both "normal" upper crust and "light" weathered crust components contributed to the source. Most samples fall in a field that can be explained by a two-component mixing between the mantle and sediment. A few samples have slightly higher δ^7Li values (approaching 0‰) and lie above the mantle-UCC mixing curve; these samples could reflect a modest contribution from an AOC-derived fluid or a less weathered sedimentary component (Fig. 4). In essence, the REE-rich alkaline melts appear to sample a hybrid source that was originally depleted SCLM but has been overprinted by recycled continental material.

Mantle heterogeneity and multiple metasomatic events

The mantle source of REE-fertile alkaline magmas is highly heterogeneous. We consider two possible scenarios to explain this heterogeneity, in light of the isotopic evidence, namely a single multi-component metasomatic event and multiple metasomatic events.

In the first scenario, a single metasomatic event introduced a diversity of materials into the mantle (e.g., mélange)[4,62]. If released over

https://doi.org/10.1038/s41467-025-66213-w

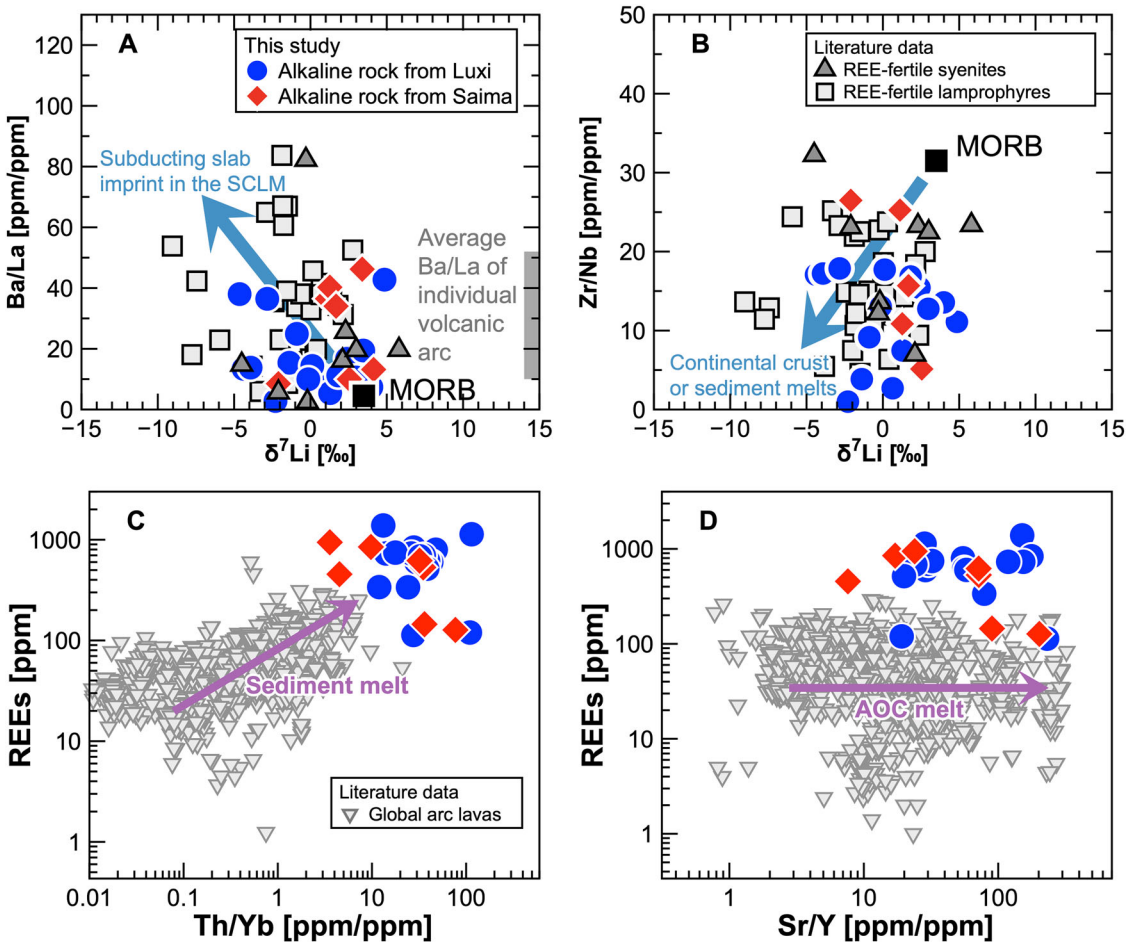

Fig. 5 | Li isotope–trace element covariations and REE concentrations in alkaline rocks. A Ba/La ratios vs. δ^7Li values, **B** Zr/Nb ratios vs. δ^7Li values, **C** REEs vs. Th/Yb, and **D** REEs vs. Sr/Y. Data sources: MORB[25,94]; REE-fertile lamprophyres[24,97]; REE-fertile syenites[67]; Ba/La ratios from individual volcanic arcs[98]. AOC altered oceanic crust, MORB mid-ocean ridge basalt. The global dataset for arc lavas is from the PetDB Database (www.earthchem.org/petdb).

a short geological interval, such diverse materials in the downgoing slab, e.g., continental and pelagic sediments as well as AOC could metasomatize the surrounding mantle during the same event. As a result, some mantle domains could be overprinted by sediment-derived material, whereas others could receive a contribution from AOC-derived material. Such a metasomatic event would create a heterogeneous mantle source.

In the second scenario, the lithospheric mantle was enriched through repeated episodes of subduction over a protracted interval of time. The eastern NCC margin experienced successive subduction events during the Phanerozoic (as discussed in the Geological background)[38]. Earlier events might have introduced ancient sediment-derived metasomatism into the lithospheric mantle (e.g., hydrous melts from subducted continent-derived sediments). Isotopic studies of the Luxi and Saima alkaline complexes have revealed elevated initial $^{87}Sr/^{86}Sr$ and very low $\varepsilon_{Nd}(t)$ values corresponding to two-stage model ages mostly around 2 Ga (Supplementary Table S5), consistent with the incorporation of Proterozoic continental material in their source. Note, the model age of the sediments is not related to the time of subduction. Subsequent subduction events (such as the Paleo-Pacific subduction) could then have introduced fresh inputs of slab fluids or melts, producing greater source heterogeneity in the Luxi complexes, particularly in $\varepsilon_{Nd}(t)$ values (Fig. 4). Over time, these episodic enrichments would have accumulated in the mantle as multiple metasomatic domains.

Despite contrasting tectonic settings (back-arc rifting at Luxi and post-collisional intrusion at Saima), both complexes display isotope signatures dominated by ancient continent-derived components. The ~110 Ma offset between their melting events indicates that mantle enrichment and melt generation were unrelated. Prolonged sediment influx and metasomatic modification preconditioned the SCLM, with later mobilization of continental materials stored in the SCLM. Because these metasomes also contain volatiles, they lower the peridotite solidus strongly and are far more fusible than the surrounding dry depleted mantle. During subsequent tectonic events, these enriched domains are the first to melt, even at very low degrees of partial melting[63]. This selective melting of enriched domains explains both the preference of REE-rich alkaline silicate systems for craton margins and their link to extensional tectonics (Fig. 1A). Thus, alkaline magmatism reflects delayed melting of a metasomatized SCLM. Subduction-related recycling produced the enrichment, whereas crustal extension triggered the melting and transferred REEs into the magmas.

Continent-derived sediments enrich the mantle sources for REE-rich alkaline magmas

The lithospheric mantle beneath Archean continental crust can act as a REE source only where subduction-related metasomatism has replenished its REE budget[1,2]. Calc-alkaline lamprophyres represent low-degree melts of the SCLM rather than the deeper asthenosphere[64]. Globally, the high REE contents and light Li isotopic compositions of orogenic lamprophyres (Fig. 5) demonstrate that melts from subducted crustal rocks can introduce significant amounts of REE and Li to metasomatized domains of the SCLM[22,65,66]. At Luxi, calc-alkaline lamprophyres accompany the syenites and have low δ^7Li and $\delta^{138/134}$Ba

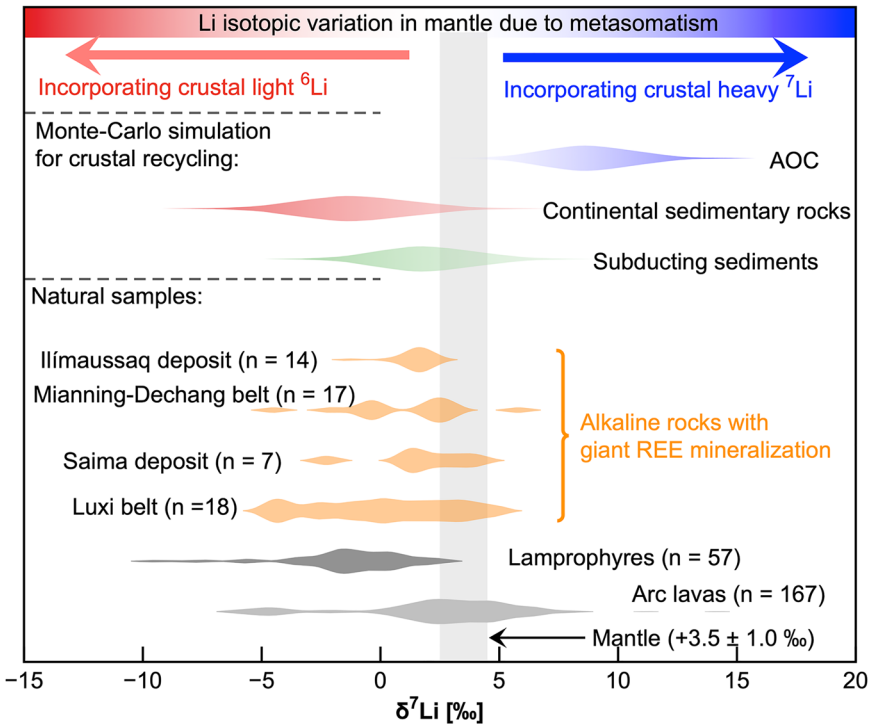

Fig. 6 | Violin plots of the Li isotopic data for arc lavas, lamprophyres, continental sedimentary rocks and alkaline rocks (REE mineralized). Also shown are the results of Monte-Carlo simulations of mantle mixing with altered oceanic crust (AOC), continental crustal materials, and subducting sediment reservoirs, respectively (for details of the modeling see Supplementary Material). Only results with a mixing ratio below 30 % (<30 % crustal materials in the mantle) are shown. The modeling results demonstrate that mantle mixing with recycled continental crust and/or sediments can reproduce the majority of the alkaline rock data. The modeling supports the hypothesis that recycling of continental crust and/or continent-derived sediments mainly controls the mantle metasomatism and enrichment of REE-fertile alkaline rocks, whereas the AOC plays a secondary role. Data sources: arc lavas[49,56,99–101]; lamprophyres[24,97]; continental sedimentary rocks[102]; alkaline rocks from the Mianning-Dechang REE belt[67]; alkaline rocks from the Ilímaussaq REE deposit[103].

values comparable to those of REE-rich syenites (Fig. 3). Taken together, the elevated Ba/La (Fig. 5A) and low Zr/Nb values (Fig. 5B), and the correlation of their isotopic signatures (low δ^{7}Li and $\delta^{138/134}$Ba in both lamprophyres and syenites; Fig. 3) strongly support continent-derived sediment metasomatism as a major source of LILE, LREE, and HFSE enrichment in the SCLM (Fig. 2). Most importantly, alkaline complexes hosting giant REE deposits such as at Luxi and Saima (NCC), Mianning-Dechang (eastern Tibetan Plateau), and Ilímaussaq (southwestern Greenland) consistently have low δ7Li values (Fig. 6), regardless of their tectonic environments (subduction-related at Luxi, post-collisional at Saima and Mianning-Dechang, and rift-related at Ilímaussaq)[10,36,67]. Furthermore, our modeling confirms that a SCLM metasomatized by recycled continental sediments adequately reproduces the observed compositional range (Fig. 6).

Across the global arc compilation, bulk REE abundances increase systematically with Th/Yb (Fig. 5C), a proxy for addition of sediment-derived melts[42,68], defining a positive trend. By contrast, REE abundances show no coherent relationship with Sr/Y (Fig. 5D), a parameter commonly used to track the evolution of magmas derived from AOC[69,70]. This decoupling implies that REE enrichment in arc magmas is governed more plausibly by the involvement of sediment-derived melts rather than by AOC-derived melts. A complementary view is that, even without extensive melting, subducted sediment can become less dense than the surrounding mantle and rise as a solid-state diapir, transporting its REE inventory[71]. These mechanisms are not mutually exclusive; both introduce REE-enriched material into the mantle and may operate in tandem.

Continent-derived sediments are heterogeneous in respect to the REE. Fine-grained shales (e.g., NASC; North American shale composite) cluster near average UCC background (~1.6×10^{2} ppm ΣREE)[72], whereas placer-type heavy-mineral sands, in which monazite/allanite are abundant, can reach >10^{3} ppm ΣREE[73,74]. The subduction of continent-derived sediments derived from weathered continental rocks is necessary to refertilize an otherwise REE-depleted mantle. During continental chemical weathering, REEs undergo strong mineralogical partitioning. In acidic, highly leached soil environments (e.g., tropical laterites), the middle to heavy REEs are relatively immobile and tend to be retained in the regolith by sorption onto secondary clay minerals like kaolinite and illite[75,76]. This forms ion-adsorption type REE deposits that are strongly enriched in MREEs and HREEs. By contrast, the LREEs are largely sequestered in some refractory detrital minerals. Accessory minerals like monazite, apatite, and bastnäsite serve as hosts for LREEs in weathered profiles[75]. These LREE-rich heavy mineral particles and clay complexes are readily eroded and transported by rivers, eventually accumulating as continent-derived sediment in subduction zones[77,78].

When REE-enriched sediments are subducted, prograde dehydration of the slab generates aqueous fluids that efficiently scavenge the most labile constituents. The REEs absorbed on clays or hosted by soluble carbonate phases (e.g., calcite/dolomite) are therefore liberated at relatively shallow levels during early devolatilization. In contrast, apatite and bastnäsite both typically release significant REE at hotter, sub-arc conditions or upon partial melting. Monazite is more refractory and requires high temperatures or partial melting to destabilize and liberate its REEs. Consequently, early slab-derived fluids are expected to carry minor REEs, consistent with experimental results[19]. At higher temperatures, silicic partial melts can dissolve LREE-bearing phases (apatite and, at higher temperatures, monazite), thereby enhancing LREE mobility[20].

Compilations show that most deep-sea REE-rich sediments exhibit pronounced negative Ce anomalies [$Ce/Ce^* = 2 \times Ce_N/(La_N + Pr_N)$][79]. For example, REE-rich bio-apatites in pelagic sediments have Ce/Ce* values ranging from 0.05 to 0.20[80]. However, ore-related alkaline magmas do not consistently display such negative Ce anomalies[79] (e.g., ~0.95 for Saima, and ~0.97 for Luxi; Supplementary Table S4). In fact, the nature of the sedimentary REE source affects Ce concentrations in the resulting magmas. Many deep-sea REE-rich sediments (biogenic apatite, early authigenic phosphates, and carbonates) acquire their REEs from seawater or pore fluids and inherit the characteristic negative Ce anomaly of seawater[79,81]. By contrast, purely detrital sediments dominated by aluminosilicate clays and oxides typically show little or no evidence of the Ce anomaly characteristic of continental crust (e.g., ~0.99 for average UCC). Furthermore, if these sediments incorporate seawater-derived carbonates or have undergone pore-water exchange, a slightly negative Ce anomaly may appear[81]. Mixing variable proportions of such continent-derived components into mantle sources therefore reproduces the observed range of Ce/Ce* in alkaline magmas.

In summary, weathering concentrates REEs into sediments, and subduction then conveys these REEs into the mantle, ultimately yielding REE-enriched magmas. The influx of these materials from the continent-derived sediments produces a metasomatized mantle source that is characteristically enriched in LILE and LREE, explaining the geochemical signatures of REE-rich alkaline rocks (Fig. 2) and some arc volcanic rocks. Our model links the weathering of the Earth's surface and subduction in the Earth's interior.

The role of plate tectonics in the critical-metal budget of the mantle

Giant REE deposits formed primarily during the Proterozoic and Phanerozoic (Fig. 1B), with a major peak at ~1.3–1.2 Ga, coeval with the assembly of Rodinia (and/or Columbia), and a smaller Paleozoic peak at ~450–400 Ma[2]. These peaks align with supercontinent cycles alternating between collisional orogenesis and extensional breakup. Geological records from the Rodinia assembly also document abundant non-arc magmas (rift- and plume-related) that were enriched in HFSEs and REEs[82]. By the Mesoproterozoic, plate-tectonic processes (e.g., prolonged subduction during the amalgamation of Rodinia) had evolved to permit extreme enrichment of these incompatible elements in the SCLM[83]. Subsequent tectonic events (whether continental rifting or collisional reactivation) could then tap into these pre-enriched mantle domains, generating the large melt volumes needed to form giant REE deposits[1,2]. In contrast, evidence of such REE-rich alkaline magmatism is scarce in the Archean, consistent with the idea that early Earth tectonics did not efficiently concentrate these elements in the mantle.

A key geodynamic inflection point was the onset of "modern" cold, deep subduction around the Neoproterozoic (after ~800 Ma)[84]. Unlike the hotter subduction of the Archean-Paleoproterozoic (which likely caused most sediments to be released at shallow depths), late Proterozoic subduction zones became cool enough to carry substantial quantities of sediments deep into the mantle[85]. Modern-style subduction thus continuously transports incompatible-element-rich sedimentary and crustal materials into the mantle wedge. Some of this recycled material is also conveyed into the deeper mantle, seeding mantle plumes and intraplate sources with enriched signatures. Crucially, silicate and carbonate melts of subducted sediments, characterized by high LREE abundances and volatile fluxing agents (CO_2, H_2O), provide prime sources for exceptionally enriched magmas tapped during rifting and orogenesis. Thus, sediment subduction is a prerequisite for the source enrichments typical of Proterozoic-Phanerozoic alkaline complexes.

A unified model

Alkaline silicate magmas associated with many REE deposits typically are the products of low-degree partial melting of a metasomatized mantle source[1,2]. Because REEs are highly incompatible, very small melt fractions can concentrate them to levels orders of magnitude higher than those produced by high-degree melting; even when the source is only modestly enriched, magmas generated by <1% partial melting may have exceptional REE contents[3]. Thus, exceptionally REE-enriched sources are not required. Equally critical is the coincidence of alkalis and volatiles in the source, which sustains REE mobility and promotes extreme differentiation (e.g., protracted fractional crystallization, liquid immiscibility), thereby amplifying REE concentrations in residual melts and/or exsolved fluids[40,41,86,87]. Consequently, an intensely metasomatized lithospheric mantle is a prerequisite for generating alkaline magmas with the potential to attain ore-forming REE concentrations during subsequent differentiation. In the case of a heterogeneously metasomatized mantle and/or a difference in the nature of the subducted material, this implies that some alkaline silicate magmas will be REE-fertile and others that are temporally and spatially associated with them will be REE-barren.

A unified model for REE-rich alkaline magmatism begins with recycled crustal material (either continental crust or continent-derived sediment) that must infiltrate and enrich the mantle tens to hundreds of millions of years prior to magmatism. This early metasomatism imparts distinct geochemical signatures (e.g., elevated Sr-Nd isotope ratios, high LREE/HREE ratios, and anomalous δ^7Li and $\delta^{138/134}Ba$ values) to the source. A second requirement is a suitable tectonic event to trigger partial melting of the enriched SCLM. In the NCC, this involved Mesozoic extension and possible lithospheric destruction[38]; in Tibet (Mianning-Dechang), Cenozoic collision and orogenic collapse[67]; and in Greenland (Ilímaussaq), anorogenic rifting[10]. Despite their differences, these settings share deep-seated fractures or thermal anomalies, enabling the metasomatized mantle to cross its solidus. Magma differentiation and emplacement govern the final REE enrichment, with prolonged melt residence, fluid exsolution, and crystal fractionation concentrating the REE to ore-forming levels[3]. To conclude, our study shows that only a pre-enriched mantle source can yield alkaline magmas capable of producing giant REE deposits, underscoring the universal significance of prior SCLM fertilization by continent-derived sediment recycling.

Methods

Major and trace element whole-rock analyses were conducted at the Lunan Geo-engineering Exploration Institute, Shandong, China. The samples were crushed to a diameter of a few centimeters and fresh pieces were selected, washed with deionized water, dried, and ground to <200 mesh for analysis. The resulting powders were then mixed with $Li_2B_4O_7$ flux (in a ratio of 1:8) and fused at a temperature of 1250 °C for major element analysis using a V8C automatic fusion machine manufactured by the Analymate Company, China. A X-ray fluorescence spectrometer (Zetium, PANalytical, XRF-1800, Shimadzu Corporation, Japan) was used for the major element analyses. Calibration was performed using both international and internal reference materials. The analytical errors for the major elements were better than 1%. Trace and rare earth element analyses were performed using ~25 mg of powder, which was dissolved in a mixture of 1 mL HF and 0.5 mL HNO_3 in screw-top Teflon beakers and left to dissolve for ~48 h at a temperature of 120 °C. A second dissolution used a mixture of 2 mL of 1:1 HCl:HNO_3 for 8 hours at 120 °C. The trace and rare earth elements were analyzed using high-resolution inductively coupled plasma mass spectrometry (ICP-MS) with an analytical precision that was typically better than 2%. The reproducibility of the concentration was determined to be better than 5%. The results of major, trace, and rare earth element analysis are reported in Supplementary Tables S3, S4.

Whole-rock analyses were performed by Nanjing FocuMS Technology Co. Ltd., Nanjing, using a Nu Plasma II multi-collector inductively coupled plasma mass spectrometer (MC-ICP-MS) to determine the Sr-Nd isotope ratios. Raw Sr and Nd isotope ratios were corrected internally for mass fractionation by normalizing to $^{86}Sr/^{88}Sr = 0.1194$ and $^{146}Nd/^{144}Nd = 0.7219$, respectively, using the exponential law. The Sr and Nd isotope ratios of the reference materials BCR-2 and AGV-2 obtained in this study (Supplementary Table S5) are consistent with published values[88].

Barium isotope ratios were determined at the University of Science and Technology of China (USTC), Hefei, China. A detailed description of the method, including sample dissolution, chemical purification, and mass spectrometric analysis, is provided in ref. 89. Isotope ratios were measured using the double-spike method in a low-resolution mode under "dry" plasma conditions. We used the international reference material NIST SRM3104a as the Ba isotope standard. The total procedural blank was 0.12 ng ($n = 4$). The Ba isotope ratios of the reference materials GSP-2 and G-2 determined in this study (Supplementary Table S5) are consistent with the published values[89]. The long-term external precision of $\delta^{138/134}Ba$ is better than ±0.05‰ (2 SD). Barium isotope fractionation is expressed relative to reference material SRM3104a using the $\delta^{138/134}Ba$ (‰) notation: $\delta^{138/134}Ba\ (‰) = [(^{138}Ba/^{134}Ba_{\ sample}/^{138}Ba/^{134}Ba_{\ standard}) - 1] \times 1000$. The results of the Ba isotope analyses are presented in Supplementary Table S5.

Lithium isotope compositions were analyzed at the Institute of Geology, Chinese Academy of Geological Sciences, Beijing, China, using a Nu Plasma II MC-ICP-MS instrument. Sample preparation and analytical procedures are described in refs. 90,91. Isotope ratios were obtained using the standard-sample-standard bracketing method and L-SVEC as Li isotope reference material. The international rock reference materials GSP-2 and BCR-2 were used to evaluate the accuracy of the determined δ^7Li values. The values obtained agree well with the published values for these reference materials (Supplementary Table S5). The 2σ long-term external precision, as determined by repeated measurements of pure Li standard solutions and sample solutions, is better than ±0.47‰[90]. Lithium isotope fractionation is expressed relative to the L-SVEC reference material using the δ^7Li (‰) notation: $\delta^7Li\ (‰) = [(^7Li/^6Li_{sample}/^7Li/^6Li_{standard}) - 1] \times 1000$. The results of Li isotope analyses are presented in Supplementary Table S5.

Data availability

All data are available in the Supplementary Material.

References

1. Beard, C. D. et al. Alkaline-Silicate REE-HFSE Systems. *Econ. Geol.* **118**, 177–208 (2023).
2. Smith, M. P. et al. From mantle to critical zone: A review of large and giant sized deposits of the rare earth elements. *Geosci. Front.* **7**, 315–334 (2016).
3. Vasyukova, O. & Williams-Jones, A. Partial melting, fractional crystallisation, liquid immiscibility and hydrothermal mobilisation – A 'recipe' for the formation of economic A-type granite-hosted HFSE deposits. *Lithos* **356–357**, 105300 (2020).
4. Kessel, R., Schmidt, M. W., Ulmer, P. & Pettke, T. Trace element signature of subduction-zone fluids, melts and supercritical liquids at 120–180 km depth. *Nature* **437**, 724–727 (2005).
5. Galvez, M. E., Connolly, J. A. D. & Manning, C. E. Implications for metal and volatile cycles from the pH of subduction zone fluids. *Nature* **539**, 420–424 (2016).
6. Hutchison, W. et al. Sulphur isotopes of alkaline magmas unlock long-term records of crustal recycling on Earth. *Nat. Commun.* **10**, 4208 (2019).
7. Chen, C., Förster, M. W., Foley, S. F. & Shcheka, S. S. Carbonate-rich crust subduction drives the deep carbon and chlorine cycles. *Nature* **620**, 576–581 (2023).
8. Hou, Z., Liu, Y., Tian, S., Yang, Z. & Xie, Y. Formation of carbonatite-related giant rare-earth-element deposits by the recycling of marine sediments. *Sci. Rep.* **5**, 10231 (2015).
9. Yang, W.-B., Niu, H.-C., Hollings, P., Zurevinski, S. E. & Li, N.-B. The Role of Recycled Oceanic Crust in the Generation of Alkaline A-Type Granites. *J. Geophys. Res. Sol. Earth* **122**, 9775–9783 (2017).
10. Hutchison, W. et al. Mantle sources and magma evolution in Europe's largest rare earth element belt (Gardar Province, SW Greenland): New insights from sulfur isotopes. *Earth Planet Sci. Lett.* **568**, 117034 (2021).
11. Mei, Q.-F., Chen, X., Yang, J.-H., Zhu, Y.-S. & Owens, J. D. Tracing Recycled Crustal Materials in the Subcontinental Lithospheric Mantle Using Thallium Isotopes. *Geophys. Res. Lett.* **49**, e2022GL099959 (2022).
12. Long, Z.-Y. et al. Heavy potassium isotopes in carbonatites reveal oceanic crust subduction as the driver of deep carbon cycling. *Sci. Adv.* **11**, eadt1023 (2025).
13. Weiss, Y., Class, C., Goldstein, S. L. & Hanyu, T. Key new pieces of the HIMU puzzle from olivines and diamond inclusions. *Nature* **537**, 666–670 (2016).
14. Rielli, A. et al. Incipient metal and sulfur extraction during melting of metasomatised mantle. *Earth Planet Sci. Lett.* **599**, 117850 (2022).
15. Qiu, K.-F. et al. Giant Mesozoic gold ores derived from subducted oceanic slab and overlying sediments. *Geochim. Cosmochim. Acta*. **343**, 133–141 (2023).
16. Qiu, K.-F. et al. The role of an oxidized lithospheric mantle in gold mobilization. *Sci. Adv.* **10**, eado6262 (2024).
17. Zhang, J.-Y. et al. Lithospheric mantle as a metal storage reservoir for orogenic gold deposits in active continental margins: Evidence from Hg isotopes. *Geology* **52**, 423–428 (2024).
18. Larsen, L. M., Rex, D. C. & Secher, K. The age of carbonatites, kimberlites and lamprophyres from southern West Greenland: recurrent alkaline magmatism during 2500 million years. *Lithos* **16**, 215–221 (1983).
19. Carter, L. B., Skora, S., Blundy, J. D., De Hoog, J. C. M. & Elliott, T. An Experimental Study of Trace Element Fluxes from Subducted Oceanic Crust. *J. Petrol.* **56**, 1585–1606 (2015).
20. Hermann, J. & Spandler, C. J. Sediment melts at sub-arc depths: an experimental study. *J. Petrol.* **49**, 717–740 (2008).
21. Foley, S. Vein-plus-wall-rock melting mechanisms in the lithosphere and the origin of potassic alkaline magmas. *Lithos* **28**, 435–453 (1992).
22. Prelević, D., Jacob, D. E. & Foley, S. F. Recycling plus: A new recipe for the formation of Alpine–Himalayan orogenic mantle lithosphere. *Earth Planet Sci. Lett.* **362**, 187–197 (2013).
23. Beard, C. D. et al. A phlogopite-bearing lithospheric mantle source for Europe's largest REE-HFSE belt: Gardar Rift, SW Greenland. *Earth Planet Sci. Lett.* **640**, 118780 (2024).
24. Krmíček, L. et al. Long-Lasting (65 Ma) Regionally Contrasting Late- to Post-Orogenic Variscan Mantle-derived Potassic Magmatism in the Bohemian Massif. *J. Petrol.* **61**, egaa072 (2020).
25. Marschall, H. R. et al. The boron and lithium isotopic composition of mid-ocean ridge basalts and the mantle. *Geochim. Cosmochim. Acta*. **207**, 102–138 (2017).
26. Wu, F. et al. Barium isotope composition of depleted MORB mantle constrained by basalts from the South Mid-Atlantic Ridge (5–11°S) with implication for recycled components in the convecting upper mantle. *Geochim. Cosmochim. Acta*. **340**, 85–98 (2023).
27. Chan, L.-H., Leeman, W. P. & Plank, T. Lithium isotopic composition of marine sediments. *Geochem. Geophys. Geosyst.* **7**, Q06005 (2006).

28. Tang, M., Rudnick, R. L. & Chauvel, C. Sedimentary input to the source of Lesser Antilles lavas: A Li perspective. *Geochim. Cosmochim. Acta*. **144**, 43–58 (2014).
29. Bridgestock, L. et al. Controls on the barium isotope compositions of marine sediments. *Earth Planet Sci. Lett.* **481**, 101–110 (2018).
30. Crockford, P. W. et al. Barium-isotopic constraints on the origin of post-Marinoan barites. *Earth Planet Sci. Lett.* **519**, 234–244 (2019).
31. Nielsen, S. G. et al. Barium isotope systematics of subduction zones. *Geochim. Cosmochim. Acta*. **275**, 1–18 (2020).
32. Wu, F., Turner, S. & Schaefer, B. F. Mélange versus fluid and melt enrichment of subarc mantle: A novel test using barium isotopes in the Tonga-Kermadec arc. *Geology* **48**, 1053–1057 (2020).
33. Wang, D., Guo, J., Romer, R. L., Liu, F. & Ouyang, D. Coeval shoshonitic and calc-alkaline mantle-derived magmatism in an ancient continental arc root. *Contrib. Miner. Pet.* **176**, 57 (2021).
34. Hao, L.-L. et al. Mg-Ba-Sr-Nd isotopic evidence for a mélange origin of early Paleozoic arc magmatism. *Earth Planet Sci. Lett.* **577**, 117263 (2022).
35. Lan, T.-G. et al. Multiple crust–mantle interactions for the destruction of the North China Craton: Geochemical and Sr–Nd–Pb–Hf isotopic evidence from the Longbaoshan alkaline complex. *Lithos* **122**, 87–106 (2011).
36. Zhu, Y.-S., Yang, J.-H., Sun, J.-F. & Wang, H. Zircon Hf-O isotope evidence for recycled oceanic and continental crust in the sources of alkaline rocks. *Geology* **45**, 407–410 (2017).
37. Zhu, Y.-S., Yang, J.-H., Sun, J.-F., Zhang, J.-H. & Wu, F.-Y. Petrogenesis of coeval silica-saturated and silica-undersaturated alkaline rocks: Mineralogical and geochemical evidence from the Saima alkaline complex, NE China. *J. Asian Earth Sci.* **117**, 184–207 (2016).
38. Wang, Y., Zhou, L., Liu, S., Li, J. & Yang, T. Post-cratonization deformation processes and tectonic evolution of the North China Craton. *Earth Sci. Rev.* **177**, 320–365 (2018).
39. Dostal, J. Rare Earth Element Deposits of Alkaline Igneous Rocks. *Resources* **6**, 34 (2017).
40. Vasyukova, O. & Williams-Jones, A. E. The evolution of immiscible silicate and fluoride melts: Implications for REE ore-genesis. *Geochim. Cosmochim. Acta*. **172**, 205–224 (2016).
41. Migdisov, A., Williams-Jones, A. E., Brugger, J. & Caporuscio, F. A. Hydrothermal transport, deposition, and fractionation of the REE: Experimental data and thermodynamic calculations. *Chem. Geol.* **439**, 13–42 (2016).
42. Pearce, J. A. Geochemical fingerprinting of oceanic basalts with applications to ophiolite classification and the search for Archean oceanic crust. *Lithos* **100**, 14–48 (2008).
43. Bai, R. et al. Barium isotopes in ocean island basalts as tracers of mantle processes. *Geochim. Cosmochim. Acta*. **336**, 436–447 (2022).
44. Kogarko, L. N., Lahaye, Y. & Brey, G. P. Plume-related mantle source of super-large rare metal deposits from the Lovozero and Khibina massifs on the Kola Peninsula, Eastern part of Baltic Shield: Sr, Nd and Hf isotope systematics. *Min. Pet.* **98**, 197–208 (2010).
45. Krienitz, M.-S. et al. Lithium Isotope Variations in Ocean Island Basalts—Implications for the Development of Mantle Heterogeneity. *J. Petrol.* **53**, 2333–2347 (2012).
46. Hofmann, A. W. Mantle geochemistry: the message from oceanic volcanism. *Nature* **385**, 219–229 (1997).
47. Ishikawa, T. & Nakamura, E. Origin of the slab component in arc lavas from across-arc variation of B and Pb isotopes. *Nature* **370**, 205–208 (1994).
48. Horner, T. J., Kinsley, C. W. & Nielsen, S. G. Barium-isotopic fractionation in seawater mediated by barite cycling and oceanic circulation. *Earth Planet Sci. Lett.* **430**, 511–522 (2015).
49. Chan, L. H., Leeman, W. P. & You, C.-F. Lithium isotopic composition of Central American volcanic arc lavas: implications for modification of subarc mantle by slab-derived fluids: correction. *Chem. Geol.* **182**, 293–300 (2002).
50. Tappe, S. et al. Sources and mobility of carbonate melts beneath cratons, with implications for deep carbon cycling, metasomatism and rift initiation. *Earth Planet Sci. Lett.* **466**, 152–167 (2017).
51. Xu, J. et al. Barium isotope fractionation during slab dehydration: Records from an eclogite-quartz vein system in Dabie orogen. *Geochim. Cosmochim. Acta*. **343**, 272–285 (2023).
52. Wunder, B., Meixner, A., Romer, R. L. & Heinrich, W. Temperature-dependent isotopic fractionation of lithium between clinopyroxene and high-pressure hydrous fluids. *Contrib. Miner. Pet.* **151**, 112–120 (2006).
53. Nan, X.-Y. et al. Barium isotope compositions of altered oceanic crust from the IODP Site 1256 at the East Pacific rise. *Chem. Geol.* **641**, 121778 (2023).
54. Gu, X.-F., Guo, S., Yu, H.-M., Xu, J. & Huang, F. Behavior of barium isotopes during high-pressure metamorphism and fluid evolution. *Earth Planet Sci. Lett.* **575**, 117176 (2021).
55. Marschall, H. R., Pogge von Strandmann, P. A. E., Seitz, H.-M., Elliott, T. & Niu, Y. The lithium isotopic composition of orogenic eclogites and deep subducted slabs. *Earth Planet Sci. Lett.* **262**, 563–580 (2007).
56. Hanna, H. D., Liu, X.-M., Park, Y.-R., Kay, S. M. & Rudnick, R. L. Lithium isotopes may trace subducting slab signatures in Aleutian arc lavas and intrusions. *Geochim. Cosmochim. Acta*. **278**, 322–339 (2020).
57. Sauzéat, L., Rudnick, R. L., Chauvel, C., Garçon, M. & Tang, M. New perspectives on the Li isotopic composition of the upper continental crust and its weathering signature. *Earth Planet Sci. Lett.* **428**, 181–192 (2015).
58. Rudnick, R. L., Tomascak, P. B., Njo, H. B. & Gardner, L. R. Extreme lithium isotopic fractionation during continental weathering revealed in saprolites from South Carolina. *Chem. Geol.* **212**, 45–57 (2004).
59. Romer, R. L. & Meixner, A. Lithium and boron isotopic fractionation in sedimentary rocks during metamorphism – The role of rock composition and protolith mineralogy. *Geochim. Cosmochim. Acta*. **128**, 158–177 (2014).
60. Gong, Y. et al. Barium isotopic fractionation in latosol developed from strongly weathered basalt. *Sci. Total Environ.* **687**, 1295–1304 (2019).
61. Nan, X.-Y. et al. Barium isotopic composition of the upper continental crust. *Geochim. Cosmochim. Acta*. **233**, 33–49 (2018).
62. Nielsen, S. G. & Marschall, H. R. Geochemical evidence for mélange melting in global arcs. *Sci. Adv.* **3**, e1602402 (2017).
63. Gülmez, F., Prelević, D., Förster, M. W., Buhre, S. & Günther, J. Experimental production of K-rich metasomes through sediment recycling at the slab-mantle interface in the fore-arc. *Sci. Rep.* **13**, 19608 (2023).
64. Krmíček, L. & Chalapathi Rao, N. V. Lamprophyres, lamproites and related rocks as tracers to supercontinent cycles and metallogenesis. In *Lamprophyres, Lamproites and Related Rocks: Tracers to Supercontinent Cycles and Metallogenesis* 0 (Geological Society of London, 2022) https://doi.org/10.1144/SP513-2021-159.
65. Vitale Brovarone, A., Alard, O., Beyssac, O., Martin, L. & Picatto, M. Lawsonite metasomatism and trace element recycling in subduction zones. *J. Metamorphic Geol.* **32**, 489–514 (2014).
66. Soder, C. G. & Romer, R. L. Post-collisional Potassic–Ultrapotassic Magmatism of the Variscan Orogen: Implications for Mantle Metasomatism during Continental Subduction. *J. Petrol.* **59**, 1007–1034 (2018).
67. Tian, S. et al. The anomalous lithium isotopic signature of Himalayan collisional zone carbonatites in western Sichuan, SW China:

Enriched mantle source and petrogenesis. *Geochim. Cosmochim. Acta*. **159**, 42–60 (2015).
68. Whalen, L. et al. Supercontinental inheritance and its influence on supercontinental breakup: The Central Atlantic Magmatic Province and the breakup of Pangea. *Geochem. Geophys. Geosyst.* **16**, 3532–3554 (2015).
69. Defant, M. J. & Drummond, M. S. Derivation of some modern arc magmas by melting of young subducted lithosphere. *Nature* **347**, 662–665 (1990).
70. Castillo, P. R. Adakite petrogenesis. *Lithos* **134–135**, 304–316 (2012).
71. Zhu, X., Liu, Y. & Hou, Z. Massive rare earth element storage in subcontinental lithospheric mantle initiated by diapirism, not by melting. *Geology* **52**, 105–109 (2023).
72. Gromet, L. P., Haskin, L. A., Korotev, R. L. & Dymek, R. F. The "North American shale composite": Its compilation, major and trace element characteristics. *Geochim. Cosmochim. Acta*. **48**, 2469–2482 (1984).
73. Sengupta, D. & Gosen, B. S. V. Placer-type rare earth element deposits. In *Rare Earth and Critical Elements in Ore Deposits* (eds, Verplanck, P. L. & Hitzman, M. W.) vol. 18 (Society of Economic Geologists, 2016).
74. Papadopoulos, A., Tzifas, I. T. & Tsikos, H. The Potential for REE and Associated Critical Metals in Coastal Sand (Placer) Deposits of Greece: A Review. *Minerals* **9**, 469 (2019).
75. Xu, C. et al. Origin of heavy rare earth mineralization in South China. *Nat. Commun.* **8**, 14598 (2017).
76. Borst, A. M. et al. Adsorption of rare earth elements in regolith-hosted clay deposits. *Nat. Commun.* **11**, 4386 (2020).
77. Kato, Y. et al. Deep-sea mud in the Pacific Ocean as a potential resource for rare-earth elements. *Nat. Geosci.* **4**, 535–539 (2011).
78. Morin-Ka, S., González-Álvarez, I., Duuring, P. & Gonzalez, C. M. Understanding rare earth elements in heavy mineral sand systems. *J. Geochem. Explor.* **274**, 107705 (2025).
79. Anenburg, M. & Liu, Y. A Global Marine Sediment Compilation and a Cerium Anomaly Perspective on Metasomatized Mantle Sources for REE-Mineralized Carbonatites. *J. Geophys. Res. Sol. Earth* **129**, e2023JB028546 (2024).
80. Deng, Y. et al. Early diagenetic control on the enrichment and fractionation of rare earth elements in deep-sea sediments. *Sci. Adv.* **8**, eabn5466 (2022).
81. Tostevin, R. et al. Effective use of cerium anomalies as a redox proxy in carbonate-dominated marine settings. *Chem. Geol.* **438**, 146–162 (2016).
82. Liu, C., Runyon, S. E., Knoll, A. H. & Hazen, R. M. The same and not the same: Ore geology, mineralogy and geochemistry of Rodinia assembly versus other supercontinents. *Earth Sci. Rev.* **196**, 102860 (2019).
83. Liu, C., Knoll, A. H. & Hazen, R. M. Geochemical and mineralogical evidence that Rodinian assembly was unique. *Nat. Commun.* **8**, 1950 (2017).
84. Stern, R. J. Modern-style plate tectonics began in Neoproterozoic time: an alternative interpretation of Earth's tectonic history. In *When Did Plate Tectonics Begin on Planet Earth?* (eds Condie, K. C. & Pease, V.) 0 (Geological Society of America, 2008), https://doi.org/10.1130/2008.2440(13).
85. Stern, R. J. Subduction Zones. *Rev. Geophys.* **40**, 3–1 (2002). 3–38.
86. Yang, W.-B. et al. Geochemistry of magmatic and hydrothermal zircon from the highly evolved Baerzhe alkaline granite: implications for Zr–REE–Nb mineralization. *Min. Depos.* **49**, 451–470 (2014).
87. Wu, M. et al. The giant Baerzhe REE-Nb-Zr-Be deposit, Inner Mongolia, China, an Early Cretaceous analogue of the Strange Lake rare-metal deposit, Quebec. *Geol. Soc. Lond. Spec. Publ.* **551**, 146 (2024).
88. Weis, D. et al. High-precision isotopic characterization of USGS reference materials by TIMS and MC-ICP-MS. *Geochem. Geophys. Geosyst.* **7**, Q08006 (2006).
89. Nan, X. et al. High-precision barium isotope measurements by MC-ICP-MS. *J. Anal. Spectrom.* **30**, 2307–2315 (2015).
90. Zhu, Z.-Y., Yang, T. & Zhu, X.-K. Achieving rapid analysis of Li isotopes in high-matrix and low-Li samples with MC-ICP-MS: new developments in sample preparation and mass bias behavior of Li in ICPMS. *J. Anal. Spectrom.* **34**, 1503–1513 (2019).
91. Duan, H.-R. et al. Purification of High Aluminum Content Samples for Rapid and Precise Analysis of Lithium Isotopes. *Spectrosc.* **44**, 198–206 (2023).
92. Van Gosen, B. S. et al. Rare-earth elements. In *Critical Mineral Resources of the United States—Economic and Environmental Geology and Prospects for Future Supply*. (eds, Schulz, K.J., DeYoung, J.H., Jr., Seal, R.R., II, and Bradley, D.C.) Professional Paper 1802, O1–O31 (U.S. Geological Survey, 2017).
93. Orris, G. J., Seo, Y., Briggs, D. A. & Cocker, M. D. Global rare earth element occurrence database. U.S. Geological Survey https://doi.org/10.5066/F7DR2TN4 (2018).
94. Sun, S. S. & McDonough, W. F. Chemical and isotopic systematics of oceanic basalts: implications for mantle composition and processes. *Geol. Soc. Lond. Spec. Publ.* **42**, 313–345 (1989).
95. Nielsen, S. G. et al. Barium isotope evidence for pervasive sediment recycling in the upper mantle. *Sci. Adv.* **4**, eaas8675 (2018).
96. Yu, H.-M. et al. Barium isotope evidence of a fluid-metasomatized mantle component in the source of Azores OIB. *Chem. Geol.* **610**, 121097 (2022).
97. Abdelfadil, K. M., Romer, R. L. & Glodny, J. Mantle wedge metasomatism revealed by Li isotopes in orogenic lamprophyres. *Lithos* **196–197**, 14–26 (2014).
98. Kelemen, P. B., Hanghøj, K. & Greene, A. R. One view of the geochemistry of subduction-related magmatic arcs, with an emphasis on primitive andesite and lower crust. *Treatise Geochem.* **3**, 659 (2003).
99. Tomascak, P. B., Ryan, J. G. & Defant, M. J. Lithium isotope evidence for light element decoupling in the Panama subarc mantle. *Geology* **28**, 507–510 (2000).
100. Magna, T., Wiechert, U., Grove, T. L. & Halliday, A. N. Lithium isotope fractionation in the southern Cascadia subduction zone. *Earth Planet Sci. Lett.* **250**, 428–443 (2006).
101. Meixner, A. et al. Lithium concentrations and isotope signatures of Palaeozoic basement rocks and Cenozoic volcanic rocks from the Central Andean arc and back-arc. *Min. Depos.* **55**, 1071–1084 (2020).
102. Romer, R. L., Meixner, A. & Hahne, K. Lithium and boron isotopic composition of sedimentary rocks — The role of source history and depositional environment: A 250 Ma record from the Cadomian orogeny to the Variscan orogeny. *Gondwana Res.* **26**, 1093–1110 (2014).
103. Marks, M. A. W., Rudnick, R. L., McCammon, C., Vennemann, T. & Markl, G. Arrested kinetic Li isotope fractionation at the margin of the Ilímaussaq complex, South Greenland: Evidence for open-system processes during final cooling of peralkaline igneous rocks. *Chem. Geol.* **246**, 207–230 (2007).

Acknowledgements

This study is financially supported by the National Key R&D Program of China (2023YFF0804200 to K.F.Q.), the National Natural Science Foundation of China (92462302 to K.F.Q.; 91962106 to K.F.Q.), the Frontiers Science Center for Deep-Time Digital Earth (2652023001 to K.F.Q.) and the Open Research Project from Shandong Provincial Lunan Geology and Exploration Institute and Shandong Engineering Research Center of Rare Elements Exploration and Comprehensive Utilization (LNY202301 to K.F.Q.). We are grateful to Fang Huang for Ba isotope

analytical assistance and to Zhi-Yong Zhu and Hao-Ran Duan for Li isotope analyses.

Author contributions

K.F.Q., Z.Y.L. and J.D. designed the project. H.C.Y. and S.S.L. conducted the experiments and chemical analyses. R.L.R., R.H., A.E. W.-J. and M.Q.W. contributed to the interpretation and discussion of the results. All authors participated in writing, reviewing, and editing the manuscript.

Competing interests

The authors declare no competing interests.

Additional information

Supplementary information The online version contains supplementary material available at https://doi.org/10.1038/s41467-025-66213-w.

Correspondence and requests for materials should be addressed to Kun-Feng Qiu, Zheng-Yu Long or Jun Deng.

Peer review information *Nature Communications* thanks Ning-Bo Li, and the other, anonymous, reviewer(s) for their contribution to the peer review of this work. A peer review file is available.